

# Shear Piezoelectricity in Poly(vinylidene fluoride-co-trifluoroethylene): Full Piezotensor Coefficients by Molecular Modeling, Biaxial Transverse Response, and Use in Suspended Energy-Harvesting Nanostructures

Luana Persano,\* Alessandra Catellani, Canan Dagdeviren, Yinji Ma, Xiaogang Guo, Yonggang Huang, Arrigo Calzolari, and Dario Pisignano

Piezoelectric materials and associated nanostructures accumulate electrical charges on their surfaces in response to an applied mechanical stress, through the change in their spontaneous electric polarization.<sup>[1,2]</sup> Exploiting deformations induced by motion, mechanical vibrations, and environmental noise,<sup>[3,4]</sup> these systems are extremely attractive for energy harvesting in information and communications technologies and personalized electronics.<sup>[5-7]</sup> Solid-state materials such as crystals<sup>[8]</sup> and ceramics<sup>[9]</sup> have been integrated in complex networks for the internet of things<sup>[10]</sup> as actuators, sensors, and transducers,<sup>[11]</sup> and as switches in memory devices. Recently, the emerging of magnetoelectric data storage,<sup>[12]</sup> self-power sources for smart wearables,<sup>[13]</sup> or implantable biomedical devices<sup>[14,15]</sup> fostered the conjugation of mechanical energy harvesting with simply shaped, biocompatible flexible materials.<sup>[16,17]</sup> In particular, the need for bendable and stretchable systems can be fulfilled with elongated nanostructures (e.g., nanowires and nanotubes).

In this framework, organics show an unequalled processing flexibility, light weight, large area, low-cost manufacturing methods, biocompatibility, and low acoustic and mechanical

impedance, which make them ideal for underwater and medical applications.<sup>[14,15,18]</sup> For instance, copolymers of vinylidene fluoride (VDF,  $[\text{CH}_2-\text{CF}_2]_n$ ) with trifluoroethylene (TrFE), are stable and can achieve a high degree of crystallinity ( $>90\%$ ).<sup>[19]</sup> In addition, they do not need to be poled because they directly crystallize from melt or solution into the ferroelectric ( $\beta$ -) phase. Piezoelectricity in these materials is related to the electronegativity difference in hydrogen and fluorine atoms, which determines an effective dipole moment in the direction normal to the carbon backbone. Consequently, these films or nanostructures are often utilized with top/bottom contacts.<sup>[20-23]</sup>

Instead, the special piezoelectric properties of polymers such as the poly(vinylidene fluoride-co-trifluoroethylene) [P(VDF-TrFE)] might lead to the development of much more versatile nanogenerator architectures. Unlike crystalline inorganic solids, for which normal piezoelectricity is generally exploited and conveniently achieved by strain along the spontaneous polarization (**P**, **Figure 1a**), in flexible polymeric systems the stress applied along one axis also causes remarkable deformations along perpendicular directions.<sup>[24]</sup> This effect, along with the reduced alignment of the polymeric chains and the presence of

Dr. L. Persano, Prof. D. Pisignano  
CNR-NANO  
Istituto Nanoscienze  
Euromediterranean Center for Nanomaterial Modelling  
and Technology (ECMT)  
via Arnesano 1, 73100 Lecce, Italy  
E-mail: luana.persano@nano.cnr.it

Dr. A. Catellani, Dr. A. Calzolari  
CNR-NANO  
Istituto Nanoscienze  
Centro S3, via Campi 213, I-41125 Modena, Italy

Dr. C. Dagdeviren  
Department of Materials Science and Engineering  
Frederick Seitz Materials Research Laboratory  
Beckman Institute for Advanced Science  
University of Illinois at Urbana-Champaign  
Urbana, IL 61801, USA

Dr. C. Dagdeviren  
The David H. Koch Institute for Integrative Cancer Research  
Massachusetts Institute of Technology  
Cambridge, MA 02139, USA

This is an open access article under the terms of the Creative Commons Attribution-NonCommercial License, which permits use, distribution and reproduction in any medium, provided the original work is properly cited and is not used for commercial purposes.

DOI: 10.1002/adma.201506381

Dr. C. Dagdeviren  
Harvard Society of Fellows  
Harvard University  
Cambridge, MA 02138, USA

Dr. Y. Ma, Dr. X. Guo, Prof. Y. Huang  
Department of Civil and Environmental Engineering  
and Department of Mechanical Engineering  
Northwestern University  
Evanston, IL 60208, USA

Dr. Y. Ma  
Department of Engineering Mechanics  
Center for Mechanics and Materials  
Tsinghua University  
Beijing 100084, China

Dr. X. Guo  
College of Aerospace and Civil Engineering  
Harbin Engineering University  
Harbin 150001, China

Prof. D. Pisignano  
Dipartimento di Matematica e Fisica "Ennio De Giorgi"  
Università del Salento  
via Arnesano, I-73100 Lecce, Italy



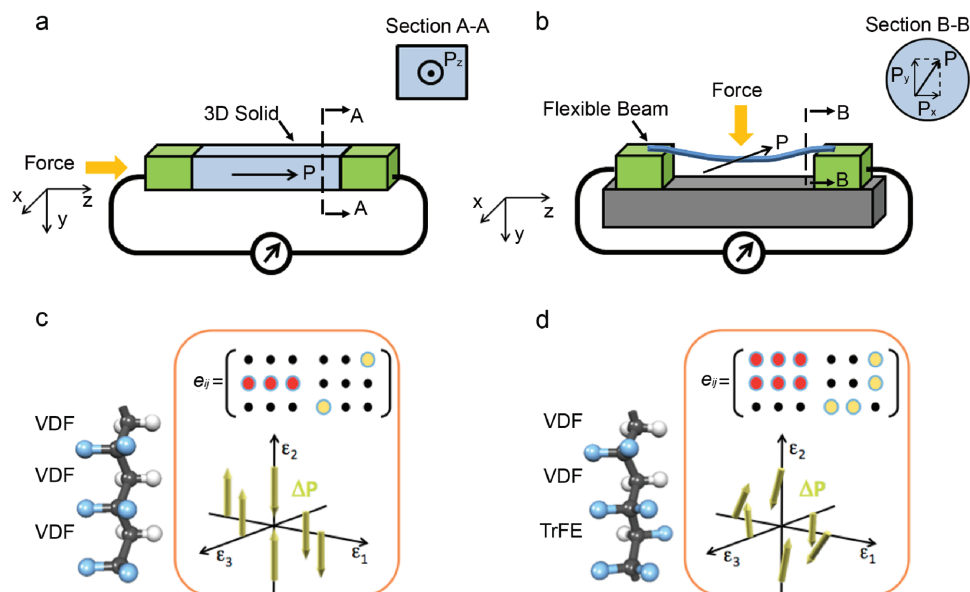


**Figure 1.** Schematics a) of typical uniaxial piezoelectricity obtained through normal strain on a 3D crystalline solid, and b) of our experimental configuration with piezoelectric P(VDF-TrFE) nanobeams, together with the corresponding cross-sectional schemes highlighting the polarization components for a generic uniaxial solid (rectangle in the top-right inset, a) and for a biaxial fiber (circle, b). The used ( $x$ ,  $y$ , and  $z$ ) coordinates are also shown in the schemes. Side view of c) VDF and d) VDF-TrFE structures, resulting from total energy and forces optimization (see the text). Dark gray, white, and cyan label, respectively, C, H, and F atoms. Green arrows define the spatial direction of polarization  $P_{\epsilon=0}$  for the minimum energy unstrained systems. Inset boxes show the corresponding sketches of piezoelectric tensors ( $e_{ij}$ ). Small (large) dots in the  $e_{ij}$  matrix plot correspond to zero (non-zero) components, whereas red (yellow) color corresponds to normal (shear) strain, respectively.

glassy grains, strips out the concept of uniaxial piezoelectricity and more complex transverse contributions are to be taken into account, in polarization and in the undergone distortions. Most studies assume only uniaxial models for polymers and organic-inorganic nanocomposites,<sup>[12,25]</sup> which may result in a limiting description of the response because of the assignment of a reduced number of piezoelectric parameters, as pertaining to systems much more symmetric than the actual ones. In this work, we demonstrate the biaxial shear activity in P(VDF-TrFE), which show the presence of two net components of the electronic polarization ( $P_x$ ,  $P_y$  according to the geometry displayed in Figure 1b) in the plane perpendicular to the chains of macromolecules. Findings reported here involve various aspects:

- (i) The full  $e_{ij}$  piezoelectric tensors and the Born effective charges due to displacement-induced polarization changes are obtained by first-principles simulations, which highlight that multiple shear components ( $e_{34}$  and  $e_{35}$ ) are non-zero in P(VDF-TrFE). Polyvinylidene fluoride (PVDF) is a 1D polar system, with poling direction along the  $y$  axis, whereas the inclusion of TrFE units strongly increases F-F repulsion and leads to the establishment of a  $P_x$  component, i.e., to a biaxial polarization character (Figure 1c,d).
- (ii) The microscopic shear is exploited in single suspended P(VDF-TrFE) nanobeams, deformed by localized bending to generate 20–40  $\mu\text{V}$  peak voltages and exhibiting high robustness and excellent adhesion at contacts.
- (iii) The resulting electromechanical behavior is also studied by means of an analytic model through the ab initio calculated piezoelectric coefficients, showing that the shear stress makes substantial contributions to the output voltage.

In the following, we report on these findings in the same order introduced above.

Our nanowires are realized by electrospinning (see the Experimental Section for details). This process is based on the elongation of a polymer flow under an intense electric field, leading to flexible filaments with ultra-high length/diameter ratio and generally circular cross section. These filaments are robust, and they can be bent repeatedly. Their polarization is mainly along a transverse direction in the plane ( $x$ - $y$  in Figure 1) perpendicular to the C backbone and to the nanowire longitudinal axis. Hence, the realization of piezoelectric generators and sensors, in which electrical signals are measured along the nanowire length, is related to shear piezoelectricity.

**Ab Initio Calculations:** The considerations above highlight the importance of a full, microscopic understanding of the piezoelectric tensor, including shear components. To this aim, we perform ab initio pseudopotential density functional theory (DFT) calculations of the piezoelectric coefficients for different copolymer configurations. Since electrospun nanowires contain thousands of polymer chains, we safely neglect surface effects and simulate filaments as bulk-like infinite systems. First, the quality of this approximation is estimated by comparing experimental and calculated infrared transmission spectra. **Figure 2** displays these spectra for fibers (continuous lines) and the theoretical results (dashed lines) for both VDF and VDF-TrFE compounds. All the fundamental features of the fibers are properly reproduced by the theoretical results, which supports the validity of the developed model. The discrepancies between the experimental and the calculated curves (such as the different spectral broadening) can be ascribed to the effect of local disorder or thermal fluctuations. For instance, considering

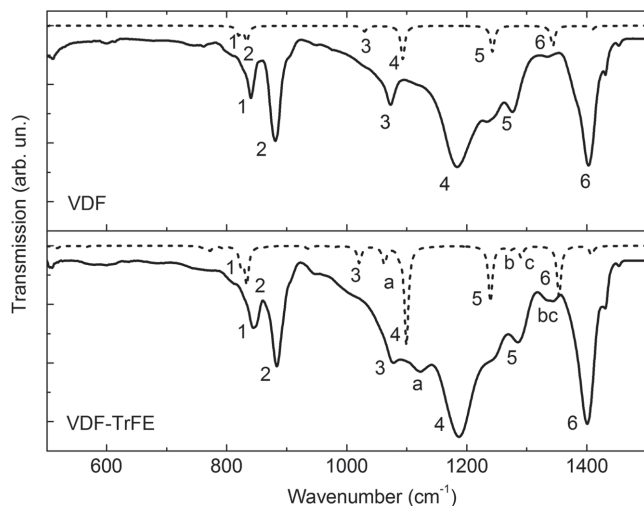


**Figure 2.** FTIR transmission spectra. Comparison of experimental (continuous lines) and theoretical (dashed lines) spectra for VDF and VDF-TrFE compounds. Numbers (1)–(6) identify spectroscopic features common to both systems ( $\approx 845$ ,  $\approx 885$ ,  $\approx 1074$ ,  $\approx 1186$ ,  $\approx 1280$ , and  $\approx 1402$   $\text{cm}^{-1}$ ), letters (a)–(c) mark vibrational peaks (1065, 1270, and 1287  $\text{cm}^{-1}$ ) associated to combined C–F and C–H rocking modes of the TrFE units. Spectra are vertically shifted for better clarity.

intra-chain disorder, as that due to the possible relative rotation of the  $\text{CF}_2$  units around the main polymer axis, may cause broader and more structured spectra (see the Supporting Information). Together with other inter- and intra-chain distortions, this finely tailors the vibrational frequencies and linewidths, thus well explaining the observed differences of experimental and calculated spectra.

The picture of the formula units of PVDF and P(VDF-TrFE) in Figure 1c,d, showing the optimized (minimum energy) structures of the two molecules, allows for a direct comparison of the dipole moments and resulting piezoelectric coefficients, as extracted by *ab initio* simulations. Symmetry arguments impose PVDF to have non-zero normal piezoelectric coefficients only along the polar ( $y$ ) axis ( $e_{21}$ ,  $e_{22}$ ,  $e_{23}$ ) and correspondingly shear coefficients for distortions in planes that do not contain this axis ( $e_{34}$ ,  $e_{16}$ ). We find that full atomic relaxation in PVDF does not break the symmetry of the system, giving rise to a uniaxial polarization ( $|P| = 0.20$   $\text{C m}^{-2}$ ), in agreement with previous theoretical reports.<sup>[18]</sup> The inclusion of TrFE units along the chain (Figure 1d), increasing F–F repulsion, imparts in-plane rotation of the monomers around the polymer axis. TrFE units have a net dipole moment, however the misalignment of the monomers along the chain leads to a global reduction of the absolute value of the polarization ( $|P| = 0.16$   $\text{C m}^{-2}$ ) and, more interestingly, to a non-zero component of the polarization along the  $x$  direction, i.e., a biaxial polarization character.

The piezoelectric response is obtained via full relaxation of the internal coordinates of the system upon applied normal and shear stress to the supercell parameters. The calculated,  $e_{ii}$  normal components of the proper piezoelectric tensor of PVDF and P(VDF-TrFE) for  $i = 1-3$  are shown in Table 1, together with the diagonal elements  $\tilde{k}_{ii}$  of the dielectric tensor, whereas the ( $e_{3i}$ ) shear components are summarized in Table 2. These findings have immediate implications for nanostructures and

**Table 1.** Calculated normal components of the proper piezoelectric tensor and of the diagonal elements of the dielectric tensor for PVDF and P(VDF-TrFE) (VDF:TrFE ratio  $\approx 70:30$ ). The  $e_{11}$  range refers to variations calculated for diluted and clustered systems (see the main text). No variation is found for other components.

	PVDF	P(VDF-TrFE)
$e_{11}$ [ $\text{C m}^{-2}$ ]	0	–0.14 to 0.05
$e_{22}$ [ $\text{C m}^{-2}$ ]	–0.32	–0.28
$e_{33}$ [ $\text{C m}^{-2}$ ]	0	0
$\tilde{k}_{11}$	2.16	2.18
$\tilde{k}_{22}$	2.14	2.17
$\tilde{k}_{33}$	2.36	2.36

devices. For perfectly crystalline PVDF nanowires lying along the  $z$  direction, only the shear coefficient  $e_{34}$ , corresponding to a solicitation along  $y$ , would contribute to the piezo-voltage collected by contacts at the opposite ends of the nanostructure. Instead, for a VDF-TrFE copolymer nanowire, one could in principle observe piezoelectric response upon solicitation along any axis in the  $x$ – $y$  plane. Furthermore, with negligible normal coefficients, i.e., with zeroing  $e_{33}$ , one would expect an insignificant contribution of stretching distortions along the nanowire axis to the overall piezoelectric response.

Since the establishment of a biaxial polarization is induced by the presence of TrFE units, it is interesting to understand how it depends on the distribution of these units along chains. We compare the structure of VDF-TrFE shown in Figure 1d, where the TrFE units are non-consecutive along the chain (configuration hereafter denoted as “diluted”), with another VDF-TrFE compound having a similar amount of TrFE units, but consecutively aligned along the chain (“clustered” model). From the calculation of the formation energy of fully relaxed systems, the diluted crystal is found to be more stable by 20 meV per monomer ( $\approx 0.5$   $\text{kcal mol}^{-1}$ ). In addition, distortions of the bonds as well as F–F interactions increase with consecutive TrFE units, and the total spontaneous polarization is significantly reduced ( $|P| = 0.02$   $\text{C m}^{-2}$ ). Finally, our calculations allow the Born effective charges,  $Z^*$ , to be obtained, quantifying the polarization changes induced by atomic displacements. Born charges provide a local contribution to changed polarization and implicitly to piezoelectric response, due to the atomic relaxation of single atoms in response to the lattice deformation (i.e., applied strain). We find that the inclusion of TrFE

**Table 2.** Calculated shear components of the proper piezoelectric tensor for PVDF and P(VDF-TrFE) (VDF:TrFE ratio  $\approx 70:30$ ).  $e_{34}$  range: calculated variations between diluted and clustered systems (see the main text). No variation is found for other components.

	PVDF	P(VDF-TrFE)
$e_{34}$ [ $\text{C m}^{-2}$ ]	0.13	0.11–0.12
$e_{35}$ [ $\text{C m}^{-2}$ ]	0	0.01
$e_{36}$ [ $\text{C m}^{-2}$ ]	0	0

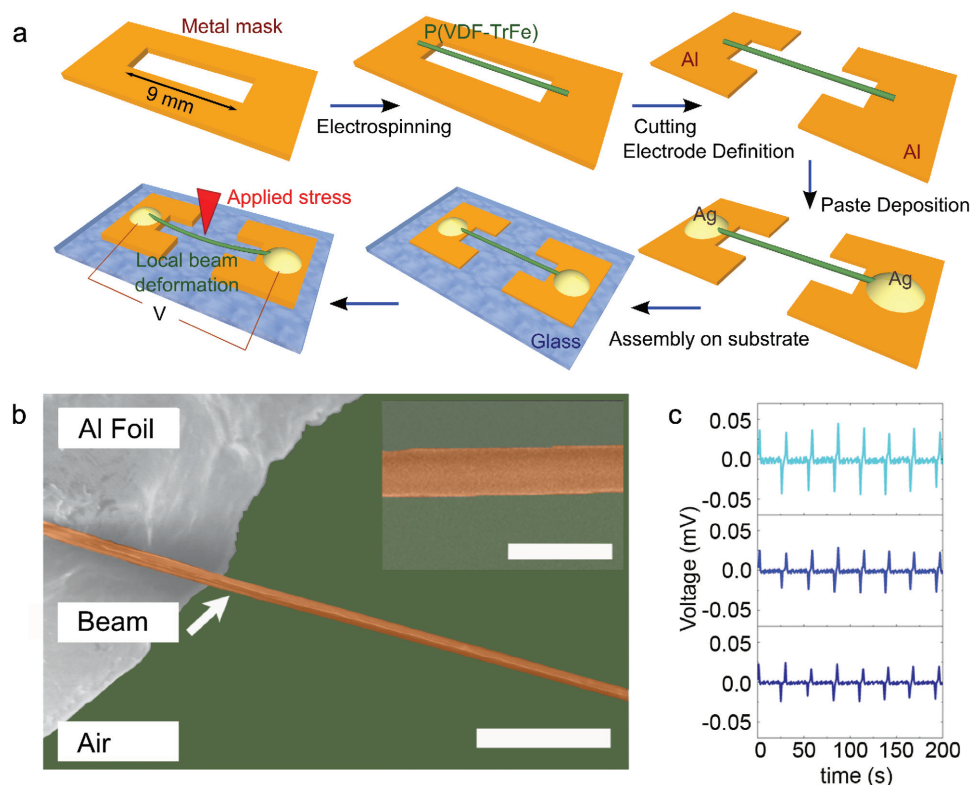


**Figure 3.** a) Process schematics illustrating the fabrication steps for piezoelectric devices based on suspended P(VDF-TrFE) nanobeams. Features not in scale. b) SEM image of a suspended piezoelectric wire with the edge lying on metal (scale bar, 5  $\mu\text{m}$ ). Inset: High-magnification image of the wire (scale bar, 1  $\mu\text{m}$ ). c) Measured output voltage under repeated load/unload cycles for the suspended wire. From bottom to top: vertical wire displacements are 38, 48, and 109 nm.

units weakly affects the absolute values of  $Z^*$ . For instance, the values of the Born charges for the  $C_H$ ,  $C_F$ , and the F atom are  $-0.28e$ ,  $+1.49e$ , and  $-0.82e$ , and  $-0.30e$ ,  $+1.43e$ , and  $-0.82e$  for VDF and VDF:TrFE, respectively, where  $e$  is the elemental charge of an electron. Further details on performed calculations and full tensor matrices are provided in the Supporting Information. Overall, simulations highlight that, due to shear piezoelectricity, bendable nanogenerators and sensors can take advantage of geometries where deformation and response do not necessarily involve the same axis.

**Single Nanobeam Piezoelectric Generator.** In order to exploit this concept, we focus on a device architecture with electrodes collecting a piezo-voltage along a direction perpendicular to the applied stress, performing experiments on individual suspended wires of P(VDF-TrFE) with average diameter of 400–600 nm. Shadow masks are used to collect the wires, which can be suspended over lengths ranging from millimeters to many centimeters on both stiff and flexible substrates carrying aluminum electrodes. The procedure to realize the devices is summarized in **Figure 3a** and involves the preparation of Al masks to be placed on a rotating collector in an electrospinning setup, the collection of single spun nanofibers across the gap realized in these masks, and the definition of electrodes by Ag paste at the two edges of suspended fibers. Following the separation of the two metallic pads, the system (Aluminum + fiber + Ag contacts) is then fixed on top of glass slides by using a bi-tape. In previous works,<sup>[26,27]</sup> piezoelectric nanofibers or nanowires have

often been used with an intimate integration with flexible substrates, namely, applying strain to those substrates which then transmit a deformation to the deposited nanostructures. Due to the needed mechanical stiffness, reports with suspended structures are largely limited to inorganic materials such as ZnO and lead zirconate titanate,<sup>[28,29]</sup> and to wires with typical length of tens to few hundreds of micrometers.<sup>[28]</sup> Here, we study a different approach, in which the strain is applied directly to a single, mm-long suspended polymer nanostructure through localized bending induced by a triboindenter tip. This implies mechanical robustness of the developed material, and optimal adhesion at contacts.

The representative scanning electron microscopy (SEM) images of the suspended wires are displayed in **Figure 3b**. The nanowires exhibit a smooth surface and uniform diameter along their entire length, and exceptionally high length/diameter ratio (up to  $5 \times 10^5$ ) in comparison with polymer nanostructures realized by other methods.<sup>[26,30–35]</sup> These electrospun materials have been found to exhibit superior piezoelectric performance,<sup>[26,36]</sup> although their operation is not fully explained by traditional models. To evaluate the piezoelectric response under specific compressive loads, flexible and thin Cu wires with a layer of silver epoxy are used to define contacts to the ends of 9 mm long polymer nanobeams. A lock-in amplifier allows the open-circuit voltage to be collected while the beams undergo well-defined levels of displacement, in sub-microscale three-point bending experiments. **Figure 3c**

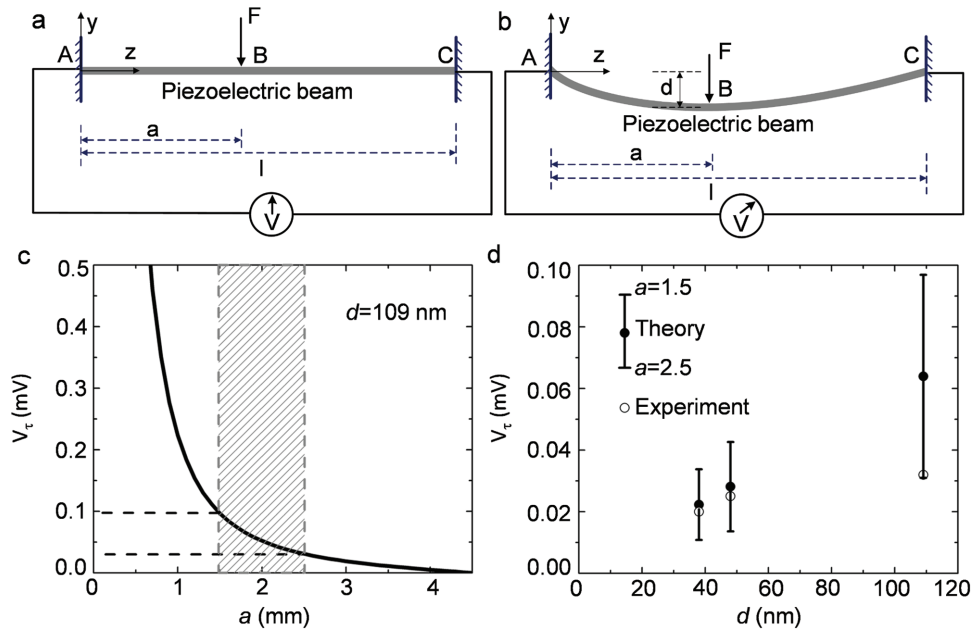


**Figure 4.** Illustration of the analytic model for the response of a suspended piezoelectric nanobeam under concentrated eccentric loading: a) undeformed and b) deformed. c) Theoretical transverse piezo-electric voltage response generated by shear stress at different positions of the bending point with  $d = 109$  nm. d) Comparison between experiment and theoretical transverse piezo-electric voltage response generated by shear stress ( $a = 1.5$ – $2.5$  mm).

shows the generated piezo-voltages during dynamic loading–unloading cycles. The periodic alternation of negative and positive peaks corresponds to the application and release of the stress. The peak output voltage generated by an individual suspended fiber increases from 20 to 40  $\mu\text{V}$  upon increasing the applied deformation (up to 109 nm along the  $y$ -direction). This evidences voltage generation from single piezoelectric polymer nanowires under a flexural deformation directly applied to the filament.

**Device Model Exploiting the Ab Initio Calculated Piezo-coefficients:** The observed behavior, particularly the transverse piezo-electric voltage generated by shear stresses, can be well explained by an analytic electromechanical model of the suspended nanostructure. **Figure 4a,b** presents a schematic illustration of piezoelectric nanobeam with both ends clamped and subjected to a concentrated eccentric loading. The beam has length  $l$ , piezoelectric and dielectric constants  $e_{ij}$  and  $k_{ij}$  [ $k_{ij} = \tilde{k}_{ij} \times \epsilon_0$ , where  $\epsilon_0$  indicates the vacuum permittivity] with  $a$  indicating the position of the applied force. We embed the  $e_{34}$  coefficient obtained by the ab initio calculations above in the electromechanical model, thus providing a coherent description of experimental findings. The resulting maximum transverse piezo-electric voltage,  $V_t$ , generated by shear stress (i.e., by taking  $e_{33} = 0$ ) is obtained as (see the Supporting Information for details)

$$V_t = \frac{3e_{34}r^2l(2a-l)(1+\nu)}{a^2(l-a)^2k_{33}}d \quad (1)$$

where  $r$  is the radius of the piezoelectric beam and  $d$  is the displacement at the loading point. **Figure 4c** shows the transverse piezo-electric voltage response at different positions of bending point obtained for  $l = 9$  mm,

$\nu = 0.35$ ,<sup>[37]</sup>  $k_{33} = 2.1 \times 10^{-11} \text{ F m}^{-1}$ ,  $e_{34} = 0.12 \text{ C m}^{-2}$ ,  $r = 300$  nm, and  $d = 109$  nm. Shear components explicitly appear in this formulation. Results show that the transverse piezo-electric voltage depends strongly on the position of the bending point ( $a$ ) making this system interesting for detecting eccentric loads and for nanoscale position sensing. Smaller  $a$  corresponds to higher transverse piezo-electric voltage. **Figure 4d** compares the voltage response obtained by experiments and theory for  $d = 38$  nm,  $d = 48$  nm, and  $d = 109$  nm. The experimental results (0.02, 0.025, and 0.038 mV for  $d = 38$ , 48, and 109 nm, respectively) are in the same range of theoretical values for  $a$  between 1.5 and 2.5 mm.

In summary, by analyzing the shear behavior, the response in suspended geometries can be fully rationalized upon taking into account transverse contributions. Given the wide use and importance of PVDF and P(VDF-TrFE) materials for the realization of nanogenerators, pressure sensors, accelerometers, and similar devices, making the full  $e_{ij}$  piezoelectric tensors available by first-principle calculations might be very useful. Indeed, multidirectional components of electronic polarization give rise to piezoelectric contributions for a large number of spatial distortions, providing polymer nanostructures with an enhanced overall piezoelectric response. The resulting architectures are extremely versatile, and they can find application in devices for nanoscale localization nearby large-scale surfaces and in systems for harvesting vibrational noise, which might activate the piezo-electric response of nanobeams without involving large-scale deformation of the underlying supporting substrates. Coupling flexural deformation and transverse piezo-electric response under compression forces establishes new rules for designing next devices based on polymer piezoelectric nanomaterials.

## Experimental Section

**Nanobeam Production and Characterization:** P(VDF-TrFE) solutions were prepared as reported in ref. [24], and placed into a 1.0 mL syringe tipped with a 27 gauge stainless steel needle. A bias of 25 kV was applied to the needle by a high voltage supply (EL60R0.6-22, Glassman High Voltage), and the solution was injected into the needle at 1 mL h<sup>-1</sup> with a syringe pump (33 Dual Syringe Pump, Harvard Apparatus). A grounded cylindrical collector (diameter 8 cm), was placed at a distance of 6 cm from the needle. Properly designed shadow masks were positioned on the surface of the disk to deposit single nanowires. Nanowires with a measured VDF:TrFE ratio of about 70:30<sup>[24]</sup> were inspected by SEM with a Nova NanoSEM 450 system (FEI), using an acceleration voltage around 5 kV and an aperture size of 30 μm. Fourier transform infrared (FTIR) spectroscopy was performed with a spectrophotometer (Spectrum 100, Perkin-Elmer Inc.) using a 4 mm wide beam incident orthogonally to the plane of the samples. FTIR measurements were performed in air at ambient conditions (temperature = 21 °C, humidity = 35%).

A triboindenter TI 950 (Hysitron) equipped with either a conospherical diamond tip (100 μm diameter) or a flat-ended cylinder sapphire tip (1 mm diameter) was used to perform load/unload cycles on suspended fibers. A maximum load of 0.5 mN was applied at a rate of 0.1 mN s<sup>-1</sup> with holding time of about 2 s. The Young's modulus of the fiber,  $E$ , is related to the obtained reduced modulus,  $E_r$ , and to the indenter properties (modulus,  $E_{IN}$ , and Poisson's ratio,  $\nu_{IN}$ ) by contact mechanics<sup>[38]</sup> as  $E_r^{-1} = (1-\nu^2)E^{-1} + (1-\nu_{IN}^2)E_{IN}^{-1}$ , where  $\nu$  is the Poisson's ratio. The modulus obtained for the electrospun wire was 2.3 GPa, in agreement with measurements on 300 nm thick films of the same material.<sup>[39]</sup> A custom data-recording system consisting of a lock-in amplifier (SR830, Standard Research Systems), a multiplexer (FixYourBoard.com, U802), and a laptop was used to capture open-circuit voltage data from the piezo-wires. An input reference signal of 1 kHz was set. The measurements were carried out at room temperature. Wires were suspended on glass substrates, with air gaps of tens of micrometers given by the thickness of the aluminum foil supporting their edges. A scheme of the used setup is reported in Figure S1 (Supporting Information).

**First-Principles Theory:** Structural and electronic properties of VDF and VDF-TrFE systems were obtained by using total-energy and forces minimization, based on PBE-GGA implementation of DFT, as coded in Quantum-Espresso.<sup>[40]</sup> Ionic potentials were described by ab initio ultrasoft pseudopotentials and single-particle wave functions were expanded in a plane-waves basis with an energy cutoff of 30 Ry. Infinite polymeric crystals were simulated using periodically repeated supercells. A (6 × 6 × 4)  $k$ -point grid was used for summations over the 3D Brillouin zone. The optimized geometries of the different systems were obtained relaxing all degrees of freedom in supercells that are multiple of formula units, further corrected via relaxation of cell volume. Supercells included six monomers arranged in two parallel chains, aligned along the  $z$ -direction, as in the predicted crystalline  $\beta$ -phase and in agreement with previous theoretical calculations.<sup>[41,42]</sup>

A van der Waals correction (Grimme formulation)<sup>[43]</sup> to dispersive forces was included to improve the description of distortion intra- and inter-chain interactions. Each structure was fully relaxed, until forces on all atoms become lower than 1 meV Å<sup>-1</sup>. Spontaneous polarization was evaluated within the Berry Phase approach.<sup>[44]</sup> Piezoelectric coefficients were obtained from finite difference derivation upon applied normal and shear cell deformation up to ±0.5%, with respect to the equilibrium parameters. In particular, the (improper) piezoelectric coefficients ( $\epsilon_{ilk} = \partial P_i / \partial \epsilon_{lk}$ ) were achieved as variations of the spontaneous polarization components ( $P_i$ ) as a function of the strain deformation ( $\epsilon_{lk}$ ). The so-called proper piezoelectric coefficients are linked to the improper ones by a simple relation which takes into account the branch phase dependence of the polarization vector (see the Supporting Information for analytical definitions).<sup>[45]</sup> Using the Voigt notation for strain indices,  $lk \rightarrow j$  [i.e., 11 → 1, 22 → 2, 33 → 3, 23(32) → 4, 13(31) → 5, 12(21) → 6], the complete proper piezoelectric response is described by an order-two tensor  $e_{ij} = \partial P_i / \partial \epsilon_{\rho}$  with  $i = 1, 2, 3$  and  $j = 1, \dots, 6$ , where

$j = 1-3$  are related to normal strain and  $j = 4-6$  to shear strain (Figure 1c,d). The dielectric tensor, Born charges ( $Z^* = -\Omega \partial P / \partial r$ , where  $\Omega$  is the unit cell volume and  $r$  indicates the coordinate of an atomic displacement), and vibrational properties (i.e., phonon eigenmodes and phonon frequency) were also determined in the regime of linear response, by using a joint finite-differences/finite-fields approaches for solid-state systems.<sup>[46]</sup> Once known phonon modes and  $Z^*$ , also the infrared cross sections could be obtained in the linear response.<sup>[47]</sup>

**Analytic Electromechanical Model:** A mechanics model of a beam with both ends clamped was established for the suspended piezoelectric wire. The model gives both the shear and normal strain distributions in the piezoelectric fiber, which together with the electromechanical analysis, provided the voltage response analytically (Supporting Information). The uniquely developed features include taking into account eccentric loads applied on the beam at given positions with respect to the fiber length, as well as the shear piezo-response.

## Supporting Information

Supporting Information is available from the Wiley Online Library or from the author.

## Acknowledgements

L.P. and C.D. thank Prof. J. A. Rogers for helpful discussion and continued support. The research leading to these results received funding from the European Research Council under the European Union's Seventh Framework Programme (FP/2007-2013)/ERC Grant Agreements No. 306357 (ERC Starting Grant "NANO-JETS"). The authors also acknowledge the EU Marie-Curie Initial Training Network Grant Agreement No. 265073 (ITN-Nanowiring) and the CNR 2015 Adjustment Program at S3/ECMT. Y.M. acknowledges the support from the National Natural Science Foundation of China (Grant No. 11402135). Y.H. acknowledges the support from NSF (CMMI-1300846 and CMMI-1400169) and the NIH (Grant No. R01EB019337).

Received: December 23, 2015

Revised: April 19, 2016

Published online: June 30, 2016

- [1] J. F. Nye, *Physical Properties of Crystals*, Oxford Science Publications, New York, USA 1957.
- [2] S. R. Anton, H. A. Sodano, *Smart Mater. Struct.* **2007**, *16*, R1.
- [3] C. Dong-Hoon, H. Chang-Hoon, K. Hyun-Don, Y. Jun-Bo, *Smart Mater. Struct.* **2011**, *20*, 125012.
- [4] K. K. Korir, G. Cicero, A. Catellani, *Nanotechnology* **2013**, *24*, 475401.
- [5] C. Dagdeviren, B. D. Yang, Y. Su, P. L. Tran, P. Joe, E. Anderson, J. Xiab, V. Doraiswamy, B. Dehdashti, X. Feng, B. Lu, R. Poston, Z. Khalpey, R. Ghaffari, Y. Huang, M. J. Slepian, J. A. Rogers, *Proc. Natl. Acad. Sci. USA* **2014**, *111*, 1927.
- [6] C. Dagdeviren, Y. Shi, P. Joe, R. Ghaffari, G. Balooch, K. Usgaonkar, O. Gur, P. L. Tran, J. G. Crosby, M. Meyer, Y. Su, R. C. Webb, A. S. Tedesco, M. J. Slepian, Y. Huang, J. A. Rogers, *Nat. Mater.* **2015**, *14*, 728.
- [7] C. Dagdeviren, Y. Su, P. Joe, R. Yona, Y. Liu, Y.-S. Kim, A. R. Damadoran, Y. A. Huang, J. Xia, L. W. Martin, Y. Huang, J. A. Rogers, *Nat. Commun.* **2014**, *5*, 4496.
- [8] C. Dagdeviren, S.-H. Hwang, Y. Su, S. Kim, H. Cheng, O. Gur, R. Haney, Y. Huang, J. A. Rogers, *Small* **2013**, *9*, 3398.
- [9] P. M. Rørvik, T. Grande, M.-A. Einarsrud, *Adv. Mater.* **2011**, *23*, 4007.

- [10] Y. Zhan, Y. Mei, L. Zheng, *J. Mater. Chem. C* **2014**, *2*, 1220.
- [11] V. Maheshwari, R. Saraf, *Angew. Chem. Int. Ed.* **2008**, *47*, 7808.
- [12] P. Martins, A. Lasheras, J. Gutierrez, J. M. Barandiaran, I. Orue, S. Lanceros-Mendez, *J. Phys. D: Appl. Phys.* **2011**, *44*, 495303.
- [13] M. Lee, C.-Y. Chen, S. Wang, S. N. Cha, Y. J. Park, J. M. Kim, L. J. Chou, Z. L. Wang, *Adv. Mater.* **2012**, *24*, 1759.
- [14] D. S. Levi, N. Kusnezov, G. P. Carman, *Pediatr. Res.* **2008**, *63*, 552.
- [15] T. I. Kim, J. G. McCall, Y. H. Jung, X. Huang, E. R. Siuda, Y. Li, J. Song, J. M. Song, H. A. Pao, R.-H. Kim, C. Lu, S. D. Lee, I.-S. Song, G. Shin, R. Al-Hasani, S. Kim, M. P. Tan, J. Huang, F. G. Omenetto, J. A. Rogers, M. R. Bruchas, *Science* **2013**, *340*, 211.
- [16] S. Egusa, Z. Wang, N. Chocat, Z. M. Ruff, A. M. Stolyarov, D. Shemuly, F. Sorin, P. T. Rakich, J. D. Jannopoulos, Y. Fink, *Nat. Mater.* **2010**, *9*, 643.
- [17] Y. Qi, J. Kim, T. D. Nguyen, B. Lisko, P. Purohit, M. C. McAlpine, *Nano Lett.* **2011**, *11*, 1331.
- [18] S. M. Nakhmanson, M. Buongiorno Nardelli, J. Bernholc, *Phys. Rev. Lett.* **2004**, *92*, 115504.
- [19] T. Furukawa, *IEEE Trans. Electr. Insul.* **1989**, *24*, 375.
- [20] S.-H. Bae, O. Kahya, B. K. Sharma, J. Kwon, H. J. Choc, B. Özyilmaz, J.-H. Ahn, *ACS Nano* **2013**, *7*, 3130.
- [21] C. Hou, T. Huang, H. Wang, H. Yu, Q. Zhang, Y. Li, *Sci. Rep.* **2013**, *3*, 3138.
- [22] J. Fang, X. Wang, T. Lin, *J. Mater. Chem.* **2011**, *21*, 11088.
- [23] K. Asadi, D. M. de Leeuw, B. de Boer, P. W. Blom, *Nat. Mater.* **2008**, *7*, 547.
- [24] L. Persano, C. Dagdeviren, Y. Su, Y. Zhang, S. Girardo, D. Pisignano, Y. Huang, J. A. Rogers, *Nat. Commun.* **2013**, *4*, 1633.
- [25] V. S. Bystrov, E. V. Paramonova, I. K. Bdkin, A. V. Bystrova, R. C. Pullar, A. L. Kholkin, *J. Mol. Model.* **2013**, *19*, 3591.
- [26] C. Chang, V. H. Tran, J. Wang, Y. K. Fuh, L. Lin, *Nano Lett.* **2010**, *10*, 726.
- [27] R. Yang, Y. Qin, L. Dai, Z. L. Wang, *Nat. Nanotechnol.* **2009**, *4*, 34.
- [28] J. Song, J. Zhou, Z. L. Wang, *Nano Lett.* **2006**, *6*, 1656.
- [29] X. Chen, S. Xu, N. Yao, W. Xu, Y. Shi, *Appl. Phys. Lett.* **2009**, *94*, 253113.
- [30] S. A. Harfenist, S. D. Cambron, E. W. Nelson, S. M. Berry, A. W. Isham, M. M. Crain, K. M. Walsh, R. S. Keynton, R. W. Cohn, *Nano Lett.* **2004**, *4*, 1931.
- [31] S. Pabba, A. N. Sclerov, S. M. Berry, M. M. Yazdanpanah, R. S. Keynton, G. U. Sumanasekera, R. W. Cohn, *ACS Nano* **2007**, *1*, 57.
- [32] P. J. Glazer, L. Bergen, L. Jennings, A. J. Houtepen, E. Mendes, P. E. Boukany, *Small* **2014**, *10*, 1729.
- [33] X. Chen, A. Li, N. Yao, Y. Shi, *Appl. Phys. Lett.* **2011**, *99*, 193102.
- [34] H. D. Espinosa, R. A. Bernal, M. A. Minary-Jolandan, *Adv. Mater.* **2012**, *24*, 4656.
- [35] J. Pu, X. Yan, Y. Jiang, C. Chang, L. Lin, *Sens. Actuators, A* **2010**, *164*, 131.
- [36] L. Persano, C. Dagdeviren, C. Maruccio, L. De Lorenzis, D. Pisignano, *Adv. Mater.* **2014**, *26*, 7574.
- [37] F. Fang, S. C. Shan, W. Yang, *J. Appl. Phys.* **2010**, *108*, 104505.
- [38] W. C. Oliver, G. M. Pharr, *J. Mater. Res.* **2004**, *19*, 3.
- [39] R. H. Kim, H. J. Kim, I. Bae, S. K. Hwang, D. B. Velusamy, S. M. Cho, K. Takashi, T. Muto, D. Hashizume, M. Uchiyama, P. André, F. Mathevet, B. Heinrich, T. Aoyama, D. E. Kim, H. Lee, J. C. Ribierre, C. Park, *Nat. Commun.* **2014**, *5*, 3583.
- [40] P. Giannozzi, S. Baroni, N. Bonini, M. Calandra, R. Car, C. Cavazzoni, D. Ceresoli, G. L. Chiarotti, M. Cococcioni, I. Dabo, A. Dal Corso, S. Fabris, G. Fratesi, S. de Gironcoli, R. Gebauer, U. Gerstmann, C. Gougoussis, A. Kokalj, M. Lazzeri, L. Martin-Samos, N. Marzari, F. Mauri, R. Mazzarello, S. Paolini, A. Pasquarello, L. Paulatto, C. Sbraccia, S. Scandolo, G. Sclauzero, A. P. Seitsonen, A. Smogunov, P. Umari, R. M. Wentzcovitch, *J. Phys.: Condens. Matter* **2009**, *21*, 395502.
- [41] N. J. Ramer, K. A. Stiso, *Polymer* **2005**, *46*, 10431.
- [42] M. Bohlén, K. Bolton, *Phys. Chem. Chem. Phys.* **2014**, *16*, 12929.
- [43] S. Grimme, *J. Comput. Chem.* **2006**, *27*, 1787.
- [44] R. Resta, D. Vanderbilt, in *Physics of Ferroelectrics: A Modern Perspective* (Eds: K. M. Rabe, C. H. Ahn, J.-M. Triscone), Springer-Verlag, Berlin/Heidelberg, Germany **2007**, Ch. 2.
- [45] D. Vanderbilt, *J. Phys. Chem. Solids* **2000**, *61*, 147.
- [46] A. Calzolari, M. B. Nardelli, *Sci. Rep.* **2013**, *3*, 2999.
- [47] X. Gonze, C. Lee, *Phys. Rev. B* **1997**, *55*, 10355.